INTERNATIONAL JOURNAL FOR NUMERICAL METHODS IN ENGINEERING
Int. J. Numer. Meth. Engng. **42**, 907–926 (1998)

TURBULENT TRANSITION SIMULATION USING THE k–ω MODEL

XIAOQING ZHENG[1,*,**,†], CHAOQUN LIU[2,‡], FENG LIU[3,§] AND CHENG-I YANG[4,¶]

[1] *Front Range Scientific Computations, Inc., CO, U.S.A*
[2] *Department of Mathematics and Statistics, Louisiana Tech University, U.S.A*
[3] *Department of Mechanical and Aerospace Engineering, University of California, Irvine, CA, U.S.A*
[4] *Hydromechanics Directorate, Carderock Division, NSWC Bethesda, MD, U.S.A*

ABSTRACT

This paper describes a novel approach in simulating laminar to turbulent transition by using two-equation models. The Total Stresses Limitation (TSL) concept is used to make the two-equation model capable of predicting high-Reynolds-number transitional flow. In order to handle the transition triggered by laminar separation at a low Reynolds number location, which commonly occurs in high speed flow, a sensor is introduced to detect separation and trigger transition in the separated zone. Test cases include the classical flat-plate turbulent boundary flow, and low-pressure turbine cascade flows at design and off-design conditions.

KEY WORDS: turbulent transition; turbulence modelling; Navier–Stokes equation

1. INTRODUCTION

Turbulent flow transition has been recognized as one of the central problems of fluid mechanics for more than a century now. It has been and still is one of the most important phenomenon in fluid flows, which have not been fully understood yet. Although the computational fluid dynamics (CFD) is now able to solve Reynolds-averaged Navier–Stokes (N–S) equations routinely, and able to simulate fully turbulent flows with reasonable accuracy, there is no reliable and economic method to determine the onset location of flow transition. Consequently, simulation of practical high Reynolds number flows could hardly meet the accuracy requirement of design community, such as less than 2 per cent error in drag prediction, and 5 per cent error in prediction of forces and moments. Without an accurate transition model, it is almost impossible to meet those stringent requirements of accuracy. Therefore development of methods for predicting flow transition is of great practical interest.

In principle, laminar flow breaks down, its subsequent development, and its eventual transition to turbulence, as well as fully developed turbulent flow can be simulated by using the Direct

* Correspondence to: Xiaoging Zheng, 34 Beecher Place, #2, Newton, MA 02159, U.S.A.
** Current address: Adina R & D, Inc., Watertown, MA 02172, U.S.A
† Research Scientist
‡ Associate Professor
§ Associate Professor
¶ Research Scientist

CCC 0029–5981/98/050907–20$17.50

Received 2 October 1996
Revised 26 November 1997

Numerical Simulation (DNS) approach. Direct numerical simulation of the whole transition process for relatively simple geometries like airfoils has been successfully carried out by Liu *et al.*[1, 2] Nevertheless, this approach is still considered too expensive even with today's supercomputers. Generally speaking, DNS has not yet developed into the stage that it can serve as a practical tool for engineering applications.

There are other ways of predicting transition based on instability theory and boundary layer theory. The most popular methods are the so-called e^n methods developed by Smith and Gamberoni[3] and by van Ingen.[4] The procedure for applying e^n methods requires three successive steps. The first step consists in the calculation of the laminar velocity and temperature profiles along the body. In the second step, the local growth rates of the unstable waves are computed for each of these profiles. This can be done by solving either the local stability equations or the Parabolized Stability Equations (PSE). Recently, the approach based on solving non-linear PSE becomes very popular since the development of unstable waves up to the weakly non-linear regime can be simulated.[5] In the third step, the local growth rates are integrated in order to determine the n factor. This method remains the most widely used method for transition prediction.[6] However, there are some major problems with using this method in practical application. First, the steady laminar solution may be not obtainable in some cases as evidenced by our last test case. Secondly, for three-dimensional flow, it is difficult to choose integration strategy for the n factor. The envelope method is widely used, but its physical meaning is not clear in many cases.[6] Furthermore, there is no 'universal' value of n factor at the onset of transition, the criteria of determining transition locations varies from case to case.

As the turbulence modelling makes steady progresses over the years and turbulent flow can be simulated quite accurately nowadays, prediction of transition via coupled solution of averaged N–S equations and turbulence model equations becomes more and more attractive. In fact, most existing low-Reynolds-number version of two-equation models can predict transition with more or less accuracy. In most cases, the transition are produced too early and too fast in comparison with the physical transition.[7] Even for the simple flat plate case, the transition locations predicted by various versions of k–ε models[8] are widely scattered and far too early. Schmidt and Patankar[9] tried to modify the production term for the k–ε model in order to match the predicted transition with the physical transition. In 1994, Wilcox presented some interesting results of simulation of transition by using his new low Reynolds number k–ω two-equation model.[10] His major efforts were made to correctly describe the transitional area. The onset of transition is controlled by means of so-called 'numerical roughness strip'. Recently, Steelant and Dick[7] presented a very interesting approach to model transitional flow by making use of the 'universal' character of the intermittency factor evolution during the transition. The N–S and turbulence model equations are conditionally averaged to include the interactive forces between laminar and turbulent phases and to make distinction between them as well. The intermittency factor is solved from a transport equation, which is derived from empirical correlations. In this way, the transition zone can be simulated with good agreement with measurements, except for the beginning of the transition. Since the transition location is one of the parameters which build up the equation for the intermittency factor, the onset of transition is actually determined by the empirical correlations just like in the so-called analytic criteria method.[6]

For practical calculations, however, determination of the onset location is much more meaningful than the description of the transitional region only. After Wilcox's work in Reference 10, efforts were made to improve the accuracy of two-equation models in predicting transition.[11, 12] Prediction of transition by two-equation models is very attractive to design engineers and CFD researchers,

since most CFD codes are incorporated with one or more kinds of two-equation models. It will be desirable if the two-equation models have the integrative ability of automatically determining transition location and modelling turbulent flows. However, from the point of view of physics, this approach is not favored simply because all spectral information is lost in the time-averaging process used by turbulence models. It is well understood now that only perturbations within a certain range of frequencies and phases are receptible to a given boundary layer (receptivity) and may trigger a turbulent transition. Therefore, conventional turbulence models, which only recognize magnitude and an averaged frequency, could not be expected to give correct answers for transitions. However, these facts do not really eradicate our expectations for two-equation models in transition prediction. Wilcox[13] has shown that spectral effects are unimportant after the initial disturbance has been amplified by a factor of only e^4. Besides, as Wilcox argued in Reference 10, 'how much more surprising is this than the great success enjoyed by the classical Smith–Van Ingen e^n method whose physical foundation is non-existent?'

Nevertheless, we cannot pretend that this approach has rigid physical foundations. But we can certainly base our modeling on the observations of experimental work and the experience of direct numerical simulation of flow transition. To some extent, this approach was justified in this work. The results achieved in this work are beyond our expectations just like sometimes the two-equation models perform surprisingly well in lots of cases.

From our experience of direct numerical simulation (DNS) of transitional flows, we noticed that wherever there is a separation, even a tiny separation bubble, the disturbance will be rapidly amplified and turbulent energy will burst. This is in conformity with experimental observation that the turbulent transition may occur at a relatively small Reynolds number if there is a separation. The existing two-equation models generally face a dilemma that they usually predict transition too early for attached flows, and too late for separated flows. Both low and high Reynolds number models are found insensitive to separation. Recently we used the total stress limitation idea to modify k–ω and k–ε models.[12] The transition position was successfully delayed to desirable Reynolds numbers for attached flows. However, the modified model failed to recognize the separation zone, and systematically predicted transition to occur too late.

It is the aim of this paper to develop a two-equation model which is able to predict transition at very high Reynolds numbers, as commonly encountered in high Reynolds number flows over smooth, slender bodies like submarines, and also to predict separation-prompted transition at low Reynolds numbers. The low-pressure-turbine-cascade flows investigated by Hodson and Dominy[14–16] are chosen as test cases because most turbomachinery flows are transitional flows. Separation-prompted transition and relaminarization frequently occur along both pressure and suction surface. Therefore, this test case provides an excellent test for the present model. Both design and off-design operational conditions are calculated and compared with experimental data. As will be shown later, the performance of the new model in simulating these test cases is excellent.

2. GOVERNING EQUATIONS AND TURBULENCE MODEL

The governing equations for compressible turbulent flows with Wilcox's low Reynolds turbulence model can be summarized as follows.[10]

Mass conservation:

$$\frac{\partial \rho}{\partial t} + \frac{\partial}{\partial x_j}(\rho u_j) = 0 \tag{1}$$

Momentum conservation:

$$\frac{\partial}{\partial t}(\rho u_i) + \frac{\partial}{\partial x_j}(\rho u_j u_i) = -\frac{\partial p}{\partial x_i} + \frac{\partial \hat{\tau}_{ji}}{\partial x_j} \tag{2}$$

Mean energy conservation:

$$\frac{\partial}{\partial t}(\rho E) + \frac{\partial}{\partial x_j}(\rho u_j H) = \frac{\partial}{\partial x_j}\left[u_i \hat{\tau}_{ij} + (\mu + \sigma^* \mu_T)\frac{\partial k}{\partial x_j} - q_j\right] \tag{3}$$

Turbulent mixing energy:

$$\frac{\partial}{\partial t}(\rho k) + \frac{\partial}{\partial x_j}(\rho u_j k) = \tau_{i,j}\frac{\partial u_i}{\partial x_j} - \beta^* \rho \omega k + \frac{\partial}{\partial x_j}\left[(\mu + \sigma^* \mu_T)\frac{\partial k}{\partial x_j}\right] \tag{4}$$

Specific dissipation rate:

$$\frac{\partial}{\partial t}(\rho \omega) + \frac{\partial}{\partial x_j}(\rho u_j \omega) = (\alpha \omega / k)\tau_{i,j}\frac{\partial u_i}{\partial x_j} - \beta \rho \omega^2 + \frac{\partial}{\partial x_j}\left[(\mu + \sigma \mu_T)\frac{\partial \omega}{\partial x_j}\right] \tag{5}$$

where t is the time, x_i the position vector, u_i the velocity vector, ρ the density, p the pressure, μ the molecular viscosity, k the turbulent mixing energy and ω the specific dissipation rate. The total energy and enthalpy are $E = e + k + u_i u_i/2$ and $H = h + k + u_i u_i/2$, respectively, with $h = e + p/\rho$, and $e = p/(\gamma - 1)\rho$. γ denotes the specific heat ratio. The other quantities are defined in the following equations:

$$\mu_T = \alpha^* \frac{\rho k}{\omega} \tag{6}$$

$$S_{i,j} = \frac{1}{2}\left[\frac{\partial u_i}{\partial x_j} + \frac{\partial u_j}{\partial x_i}\right] \tag{7}$$

$$\tau_{i,j} = 2\mu_T\left[S_{i,j} - \frac{1}{3}\frac{\partial u_k}{\partial x_k}\delta_{i,j}\right] - 2/3\rho k \delta_{i,j} \tag{8}$$

$$\hat{\tau}_{i,j} = 2\mu\left[S_{i,j} - \frac{1}{3}\frac{\partial u_k}{\partial x_k}\delta_{i,j}\right] + \tau_{i,j} \tag{9}$$

$$q_j = -\left(\frac{\mu}{Pr_L} + \frac{\mu_T}{Pr_T}\right)\frac{\partial h}{\partial x_j} \tag{10}$$

where Pr_L and Pr_T are the laminar and turbulent Prandtl numbers, respectively. The closure coefficients are

$$\alpha^* = \frac{\alpha_0^* + Re_T/R_k}{1 + Re_T/R_k} \tag{11}$$

$$\alpha = \frac{5}{9}\frac{\alpha_0 + Re_T/R_\omega}{1 + Re_T/R_\omega} \tag{12}$$

$$\beta^* = \frac{9}{100}\frac{5/18 + (Re_T/R_\beta)^4}{1 + (Re_T/R_\beta)^4} \tag{13}$$

$$\beta = 3/40, \quad \sigma = 1/2, \quad \sigma^* = 1/2 \tag{14}$$

$$\alpha_0^* = \beta/3, \quad \alpha_0 = 1/10 \tag{15}$$

$$R_k = 6, \quad R_\omega = 2{\cdot}7, \quad R_\beta = 8 \tag{16}$$

where Re_T is the turbulence Reynolds number defined by:

$$Re_T = \frac{\rho k}{\omega \mu} \tag{17}$$

3. NUMERICAL METHODS

The above-described governing equations are solved by finite volume methods developed by Liu and Zheng.[17, 11] This method, with the combination of cell-centred and cell-vertex scheme, strongly couples the k–ω and N–S equations together, and maintains a small stencil for all diffusion terms. Another advantage of this method is that the computations of the diffusive terms only cost half for 2-D and one-third for 3-D as that of other compact schemes which evaluate the diffusive terms at cell interfaces. This significantly improves the computational efficiency. For completeness, the basic idea of the staggered finite volume method is outlined here.

After the computational domain is discretized into a number of quadrilateral cells in two dimensions or hexahedral cells in three dimensions, the governing equations are applied to each of the cells in integral form. For simplicity, consider a computational mesh in two dimensions. With a cell-centred scheme the flow variables ρ, ρu_i, and ρE are defined at the cell centres marked by the circles in Figure 1. Both the convective and diffusive fluxes in the N–S equations have to be estimated over the four cell faces of a control volume, for example, the cell Ω shown in Figure 1. The convective fluxes can be easily estimated by taking the averages of the flow variables on either side of a cell face, yielding a five-point stencil for the total Euler flux balance. For diffusion terms, which involve second derivatives of control variables, both cell-centred and cell-vertex schemes are used to reduce the stencil and establish direct connection between k–ω and N–S equations. First, a staggered auxiliary control volume Ω' was formed by connecting the cell centres and the mid-points of the cell faces. Since the flow variables are defined at the vertices of this auxiliary cell, Gauss's formula can then be applied as in a vertex scheme to calculate the velocity and temperature gradients at the centre of the auxiliary cell, which in fact is the vertex of the original cell Ω. Once the stresses are known at the cell vertices of Ω, the diffusive fluxes in the N–S equations can then be easily evaluated over the cell faces by trapezoidal rule as in a vertex scheme. This yields a compact discretization stencil involving only nine points with minimum spatial extent as shown by the circles in Figure 1.

For the k–ω equations, the control variables k and ω are not defined at cell centres. Instead, they are defined at cell vertices marked by the crosses. If k and ω were defined at the cell centres, one would have to interpolate the strain tensor calculated at the cell vertices to the cell centre, so that the production terms for the control volume can be evaluated. On the other hand, the eddy viscosity μ_T calculated from the k and ω at the cell centres must be translated to the cell vertices in order to calculate the turbulent stresses there. This double averaging process would broaden the final discretization stencil for the coupled N–S and k–ω equations, and thus reduce the accuracy and increase the likelihood of uninhibited growing modes.

Based on the above reasons, the k–ω equations are integrated over the staggered control volume Ω'. They are discretized in a similar way to the N–S equations, only in the reverse order of using the original and the auxiliary cells. This staggered control volume strategy, in fact, seems to be a

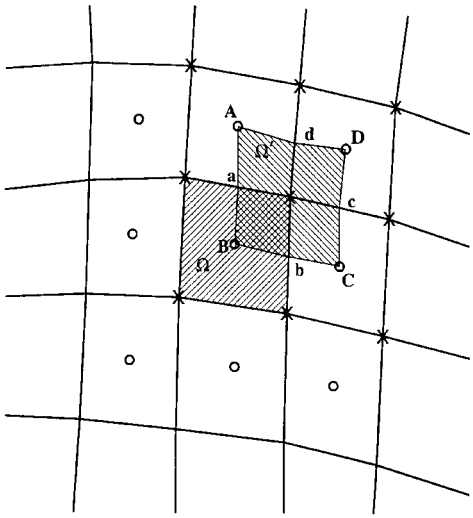

Figure 1. Staggered control volumes for a mixed cell-centre and cell-vertex scheme

natural way to couple the N–S and k–ω equations. We will no longer need the excessive averaging steps for the strain tensor and the eddy viscosity. The production terms are evaluated at exactly the same locations, namely the cell vertices, where the stress and strain tensors are calculated, and the eddy viscosities calculated from k and ω at these cell vertices are directly used to calculate the turbulent stress tensors. In this way, the N–S equations and the k–ω equations in their discrete forms are coupled as closely as possible. The discretization of each set of the equations involves a stencil of only nine points.

The accuracy of this method is formally second order on a smooth grid. Although the convective terms of the turbulence model equations are discretized by using a third-order upwind-biased high-resolution scheme, the N–S equations are discretized by using both a third-order Roe's upwind scheme[18] and the Jameson's second-order central difference scheme with adaptive dissipation.[19] Since no significant difference was found between the results with use of Roe's upwind scheme and with use of Jameson's central difference scheme in our test cases, all the results reported in this paper were obtained with Jameson's second-order central difference scheme. Only fourth-order dissipation is used since all our test cases are subsonic flows.

After performing spatial discretization, the governing equations are reduced to a set of ordinary differential equations with only derivatives in time, which can then be solved by using a hybrid multi-stage scheme. Residual smoothing and multigrid methods are used to accelerate convergence of the calculation. Details can be found in References 17 and 11.

This approach has proved extremely efficient for solving Reynolds-averaged N–S equations and two-equation models when multigrid methods are applied to both sets of equations.[20]

4. TOTAL STRESS LIMITATION

In Reference 11, a modification to the k–ω model is proposed to alleviate its strong dependency on far field values of ω, and also to account for the transport effects of the total (include the principal, of course) turbulent shear-stress. It was also found it can be used to control turbulent transition. Although the modification is proposed for k–ω model, it can also be used for the k–ε model.

The development of the modification is here described. First, from the definition of the turbulence kinetic energy

$$k = \tfrac{1}{2}(\overline{u'^2} + \overline{v'^2} + \overline{w'^2}) \tag{18}$$

we have

$$(2k)^2 = \overline{u'^2}^2 + \overline{v'^2}^2 + \overline{w'^2}^2 + 2(\overline{u'^2}\,\overline{v'^2} + \overline{v'^2}\,\overline{w'^2} + \overline{u'^2}\,\overline{w'^2})$$

Since

$$\frac{1}{\rho}\Sigma\hat{\tau}_{i\cdot j}^2 = \overline{u'^2}^2 + \overline{v'^2}^2 + \overline{w'^2}^2 + 2(\overline{u'v'}^2 + \overline{v'w'}^2 + \overline{u'w'}^2)$$

and

$$\overline{u'v'} \leqslant \sqrt{\overline{u'^2}\,\overline{v'^2}} \tag{19}$$

we therefore have

$$\sqrt{\Sigma\hat{\tau}_{i,j}^2} \leqslant 2\rho k \tag{20}$$

By using the Boussinesq constitutive assumption

$$\hat{\tau}_{i,j} = 2\mu_t\left[s_{i,j} - \frac{1}{3}\frac{\partial u_k}{\partial x_k}\delta_{i,j}\right] - \frac{2}{3}\rho k\delta_{i,j} \tag{21}$$

where

$$s_{i,j} = \frac{1}{2}\left(\frac{\partial u_i}{\partial x_j} + \frac{\partial u_j}{\partial x_i}\right) \tag{22}$$

the relation (20) can be rewritten as

$$\sqrt{\left[2\mu_t\left(s_{i,j} - \frac{1}{3}\frac{\partial u_k}{\partial x_k}\delta_{i,j}\right) - \frac{2}{3}\rho k\delta_{i,j}\right]^2} \leqslant 2\rho k \tag{23}$$

which can be reduced to

$$\begin{aligned}\omega &\geqslant \phi\alpha^*\sqrt{2\left(s_{i,j} - \frac{1}{3}\frac{\partial u_k}{\partial x_k}\delta_{i,j}\right)\frac{\partial u_i}{\partial x_j}} \\ &= \phi\alpha^*\sqrt{\text{velocity strain}}\end{aligned} \tag{24}$$

where $\phi = \sqrt{3}/2$.

The above constraint is incorporated into the k–ω model by redefining ω as

$$\omega = \max(\omega_o, \phi\alpha^*\sqrt{P_d}) \tag{25}$$

where ω_o is the solution from Wilcox original k–ω model, P_d is the exact velocity strain included in the production term of turbulence model, which is directly available, no extra calculations are needed.

From the above, we know ϕ has a definite value of $\sqrt{3}/2$, which represents the least requirement from the realizability of the turbulence model. Essentially, the starting equation (20) can be regarded as a limit on the portion of deviant turbulent stress. Experimental data reveal that the portion of deviant turbulent stresses is actually much lower, for instance $\tau_{i,j} \leqslant 0{\cdot}3\rho k$ was found in many cases. If we start from this relation instead of the equation (20), then we will end up with a much larger value of ϕ. This suggests that more severe limit on ω should be imposed. Since the resultant equation (24) sets a lower limit for turbulence dissipation rate, ϕ can be used as a direct and effective tool to control turbulent energy growth. In fact, it has been found for most cases, $\phi = 2{\cdot}5$ can yield satisfactory prediction of transition. The modification was also found to have very little effect on the accuracy of k–ω model in fully turbulent regions, as long as $\phi < 3{\cdot}1$.

5. SEPARATION-AWARE MODEL

As will be shown later, the above modification can significantly improve the ability of k–ω model in predicting transition. However, in common with other two-equation models, it ignores the effects of boundary layer separation. It can be shown that in the separation zone, the magnitude of velocity strain, which constitutes the turbulence production, is generally the same order as in the non-separated area. However, direct numerical simulation (DNS) of transitional flows reveals that wherever there is a separation, even a tiny separation bubble, the disturbance will be amplified rapidly and the turbulent energy will burst. This is also confirmed by many experiments. Usually, the turbulent transition will occur at a relatively small Reynolds number if there are separations. Therefore, a further modification is needed to account for separation effects.

First, we need to devise a sensor which can detect separation. It must be able to distinguish the vorticity of separation from the vorticity of shear layer. High-order derivatives should be avoided since they are too expensive to calculate. Generally, a separation zone is characterized by streamlines with large curvature, and this distinct feature is used to construct the separation sensor.

For two-dimensional flow, the curvature of a streamline can be derived straightforwardly from its definition as

$$C_s = \frac{\left| u\left(u\frac{\partial v}{\partial x} + v\frac{\partial v}{\partial y}\right) - v\left(u\frac{\partial u}{\partial x} + v\frac{\partial u}{\partial y}\right)\right|}{(u^2 + v^2)^{3/2}} \tag{26}$$

The general form of streamline curvature in three-dimensional flow, though a little more complicated, can be derived as follows.

Set $\mathbf{n}_q = u/q, v/q, w/q$, where $q = \sqrt{u^2 + v^2 + w^2}$, is the velocity magnitude, then we can prove the differential of $\mathbf{n}_q$ along a streamline s can be expressed as:

$$\frac{\partial \mathbf{n}_q}{\partial s} = (\mathbf{n}_q \cdot \mathrm{grad})\mathbf{n}_q = \frac{1}{q}\mathbf{q} \cdot \nabla\left(\frac{\mathbf{q}}{q}\right)$$

$$= \frac{1}{q^2}(\mathbf{q}\cdot\nabla)\mathbf{q} - \frac{\mathbf{q}}{q^3}(\mathbf{q}\cdot\nabla q)$$
$$= \{q(\mathbf{q}\cdot\mathrm{grad})\mathbf{q} - \mathbf{q}[\mathbf{q}\cdot\mathrm{grad}(q)]\}/q^3 \tag{27}$$

where $\mathbf{q} = (u, v, w)$, is the velocity vector.

Therefore, the magnitude of the curvature can be calculated as:

$$C_\mathrm{s} = \left|\frac{\partial \mathbf{n}_q}{\partial s}\right| = \frac{1}{q^2}\sqrt{C_x^2 + C_y^2 + C_z^2} \tag{28}$$

where

$$C_x = \mathbf{q}\cdot\mathrm{grad}(u) - \frac{u}{q}(\mathbf{q}\cdot\mathrm{grad}(q)) \tag{29}$$

$$C_y = \mathbf{q}\cdot\mathrm{grad}(v) - \frac{v}{q}(\mathbf{q}\cdot\mathrm{grad}(q)) \tag{30}$$

$$C_z = \mathbf{q}\cdot\mathrm{grad}(w) - \frac{w}{q}(\mathbf{q}\cdot\mathrm{grad}(q)) \tag{31}$$

It can be verified that equation (28) will reduce to equation (26) if $w = 0$.

C_s can be regarded as a measure of vortex length, which in fact is the inverse of vortex radius. The non-dimensional parameter, which turns out to be an excellent separation indicator, is defined as

$$S_l = \frac{C_\mathrm{s}\sqrt{k}}{\omega} \tag{32}$$

The physical meaning of S_l is the ratio of turbulent length (time) scale to the vortex length (time) scale, or can be interpreted as the ratio of the production between turbulence and vortex to the turbulence dissipation.

With help of S_l, the separation-aware model can be constructed by modifying (11) to

$$\alpha^* = \frac{\alpha_0^* + \alpha_1^* + Re_\mathrm{T}/R_k}{1 + Re_\mathrm{T}/R_k} \tag{33}$$

where

$$\alpha_1^* = C_0\frac{R_l}{\frac{1}{10} + R_l} \tag{34}$$

$$R_l = \frac{S_l}{\sqrt{Re_\mathrm{T}}} = C_\mathrm{s}\sqrt{\frac{\mu}{\rho\omega}} \tag{35}$$

$\alpha_0^*, Re_\mathrm{T}$, and R_k are the same as defined in Wilcox's original low-Reynolds-number model. α_1^* is introduced to trigger transition when S_l reaches a certain value. It is the only new term of the proposed model. The modification proved insensitive to the constant C_0 in equation (34). In fact, our calculation shows that the proposed model performs almost the same for $C_0 = 10$–14. Generally, $C_0 = 13$ is recommended.

Although the modification is minor compared to the complexity of the original low-Reynolds model, it proved very effective in allowing the two-equation model to react promptly to laminar separation. It only takes effect in laminar separation zones. Once the flow becomes turbulent, Re_T in equation (33) will take over, and the effect of the modification will disappear. The best

result can be achieved if this modification is combined with the TSL technique by setting ϕ in equation (25) to 2·5. From the test cases that have been carried out so far, it has been found that the modifications significantly improve the performance of the turbulence model in predicting turbulent transition.

6. BOUNDARY CONDITIONS

The boundary types encountered in this work are classified as solid wall, periodic, inflow and outflow. For viscous flow, a non-slip condition is imposed on the solid wall boundary by setting the flow velocity equal to that of the body, and zero pressure gradient normal to the surface is specified to determine the pressure on the wall.

One of the great advantages of the k–ω model over other two-equation models is the simplicity of treatment of wall boundary conditions. The k–ω model does not require damping functions in viscous sub-layer and no normal distance from wall needs to be defined except only for the first point. Since the closure parameters of k–ω model have been tuned to enable the model to accurately reproduce the wall-function law in near wall regions, no explicit logarithmic wall functions are needed in the wall boundary conditions even for the high-Reynolds-number k–ω model.

The turbulent mixing energy k is set to zero at the wall. The specific dissipation rate ω does not have a natural boundary condition for its value at wall is infinite. In our calculations, the boundary condition of ω is actually imposed at the first point away from the wall. Following the asymptotic solution by Wilcox, the ω value at the first point is defined as

$$\omega_1 = \frac{6\nu_w}{\beta y^2} \tag{36}$$

Its value at the wall is found numerically from our difference scheme to ensure that the interpolated value of ω at the near wall surface of the first control volume for the ω equation also satisfies the asymptotic solution when the normal convective velocity is positive in the direction toward to the second point from the wall, thus

$$\omega_0 = \frac{19}{9}\frac{6\nu_w}{\beta y^2} \tag{37}$$

In the near wall region, the ω equation is dissipation-dominant, and ω decays very rapidly from the wall distance as shown in equation (36). During the multigrid cycle, the coarser grids could not resolve such a great variation. Therefore, the ω at the wall and the first point are passed down without updating on each coarse grid level.

Since a ghost cell is introduced to store the value and derivatives across the boundary, the boundary conditions for periodic interfaces are easily accomplished by assigning the ghost cell with the values of corresponding cells.

At the inlet boundary, the total enthalpy, total pressure, and the flow angles are specified for subsonic inlet flow. After the velocity magnitude is extrapolated from inside the flow field, all the flow variables on the boundary can be found. For supersonic inlet flow, all flow variables are specified. The freestream values of ω is estimated by using the following equation as suggested by Menter[21]

$$\omega_\infty = \mathcal{O}\left(10\frac{U_\infty}{L}\right) \tag{38}$$

The turbulent kinetic energy k is determined from the inflow turbulent intensity. Since transition is very sensitive to the inflow turbulent energy, the measured free stream turbulent intensity is used in this work to determine the boundary value of k.

7. COMPUTATIONAL RESULTS

First, the classical flat plate boundary layer is calculated to validate the turbulence model and coding. A grid of 96×64(cells) is used, with 16 points before the plate leading edge, 73 points on the plate and eight after. Sixty-five points are placed in the normal direction and stretched out to far field from the plate surface. The original high-[22] and low-Reynolds-number versions of the k–ω model[10] are also used in this study. Without modification, all of the k–ω models (and the k–ε model too) predict transition to turbulence at Reynolds numbers which are at least an order of magnitude too low comparing with experimental data.[23] The inflow turbulence intensity is set to a very low level($Re_T = 0{\cdot}001$). Therefore, very late transition is expected. Figure 2 shows the skin friction calculated by these two models and with our modifications. Without modification, the original k–ω model will give a very early transition prediction. By choosing different values of ϕ in equation (25), the transition point can be controlled over a quite wide range. However, there is a flat region between approximately $\phi = 1$ and 2, which means the results will remain unchanged if ϕ varies between one and two. A remarkable feature of this modification is that it does not affect the solution of turbulent region for $\phi \leqslant 3{\cdot}1$ as concluded in previous study. No matter where the transition occurs, the calculated skin friction coefficient follows closely Blasius' laminar-boundary-layer solution before transition, and then Prandtl's one-fifth law afterwards.

However, the delay of transition with use of TSL is limited. Larger values of ϕ will completely prevent turbulent transition. It is true that the common transition Reynolds number is between 10^4 and 10^5 for flat-plate flow, which is in a range that TSL is capable of handling. However if the inflow is quiet enough, the transition Reynolds number can be as high as 10^6, which is beyond TSL's capability. In order to further delay the transition to turbulence and maintain accuracy in fully turbulent regions, a modification to low-Reynolds-number k–ω model is required.

Nevertheless, the TSL modification is considered very important. First, the transition in practical flows is usually much later than that predicted by standard k–ω and k–ε models as well as the low-Reynolds number versions of those models. Additional measures are needed to further delay the transition. Second, even though the transition can be postponed through adjusting the coefficients in the low-Reynolds number k–ω model, we found it is too sensitive to the solution process. A disturbance from the iteration procedure could cause transition to occur too early. This solution still belongs to one of the many solutions of governing equations, because the highly nonlinearity of the governing system. Therefore, the multigrid method cannot be used in the solution of the low-Reynolds number k–ω model since the corrections from coarse grids can bring in disturbance and cause incorrect transition. However, when the TSL modification is used, the transition is not sensitive to the solution methods any more. The transition is only governed by the parameter ϕ and the inflow turbulence intensity in conformity to the physics. Therefore, the modified equation system can be subjected to acceleration techniques, such as multigrid, which has been proved extremely efficient.

The second test case concerns turbine cascade flows at two operational conditions, as tested and analyzed by Hodson and Dominy.[14–16] At its design condition this cascade has an exit isentropic Mach number of 0·7 and an incidence angle of 38·8°. The experimental Reynolds number based

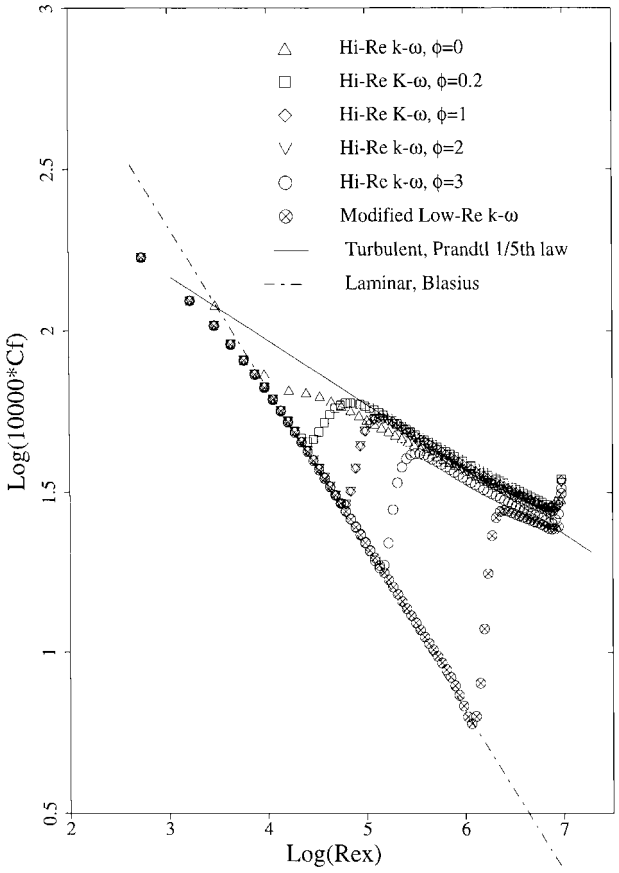

Figure 2. Skin friction coefficients of flat plate flow. $Re_\infty = 10^7$, parameter study for k–ω models with TSL

on exit velocity and blade chord length is $2{\cdot}9 \times 10^5$. The inlet turbulence intensity is 0·5 per cent. Although the blade is linear, the side walls have a 6° divergence. Therefore, a purely two-dimensional calculation would under-predict the isentropic Mach number on the forward part of the blade for the same exit Mach number. In order to avoid such a discrepancy, a stream tube thickness correction is incorporated in the calculation of the Euler fluxes.[17, 11]

Four different sizes of grids, $96 \times 40, 160 \times 64, 192 \times 80$ and 224×96, are used in this study. Most results reported here are calculated on the grid of 192×80. The distance from the first point to the wall is kept within $y^+ = 1$.

In Figure 3, the calculated isentropic Mach number distributions under design conditions by the high-Reynolds-number k–ω model,[22] low-Reynolds-number k–ω model,[10] and the present transitional model are plotted against experimental data, respectively. Good overall agreement with experimental data is achieved by all three turbulence models. However, the first two models fail to capture a small hump in the isentropic Mach number distribution on the back of the suction surface. As observed in experiment,[14] the small hump was due to a laminar separation bubble. The flow becomes turbulent only after it has separated and before it re-attaches under influence

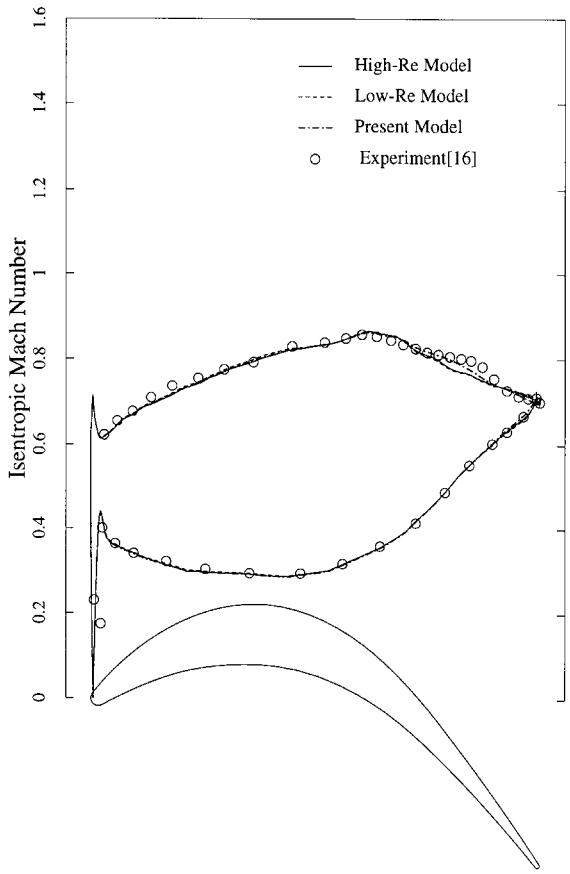

Figure 3. Isentropic Mach number distribution at design condition

of turbulence. Both high and low-Reynolds-number k–ω models predict transition too early and fail to predict the separation bubble. The new model basically captures the small hump in the isentropic Mach number distribution as shown in Figure 3, but there are still noticeable differences between the shape of the hump captured by the prediction and shown by the measurement data. The flow within the small separation bubble is so delicate that any minor deficiency of grid resolution or turbulence model could cause such differences. Anyway, even on a grid of 192×80, which is considered very fine for cascade flow computation, the separation strength (measured by the magnitude of negative skin friction) is still slightly under-predicted. When the grid is refined to 224 along flow direction and 96 in blade-to-blade direction, the small hump in the isentropic Mach number distribution becomes more obvious as shown in Figure 4. A concave variation following the hump is fully captured.

Figures 5 and 6 show the skin friction distributions on the pressure and suction surface normalized by the exit dynamic pressure. The original high-Reynolds-number k–ω model predicts transition too early and therefore over-predicts the skin friction. The-low-Reynolds number k–ω model gives correct transition and relaminarization after a tiny separation bubble on each of

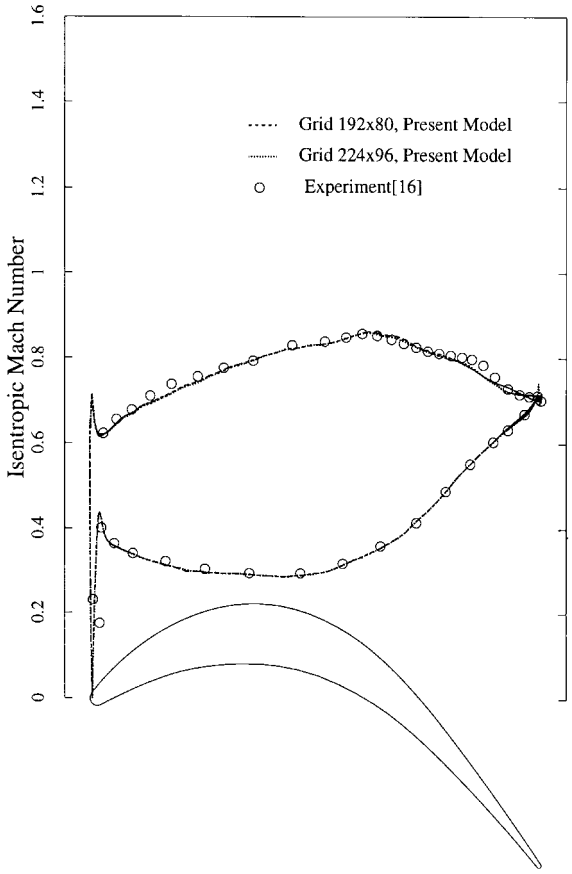

Figure 4. Mesh resolution effects on separation bubble prediction

pressure and suction sides, but it still gives a too early transition location on the suction surface. As a result, it misses the small laminar separation bubble on the back of the suction surface just like the high-Reynolds-number k–ω model does. With use of TSL and separation-aware modifications, the transition position and the relaminarization are predicted accurately. The boundary layer solution[14] is plotted in the same figure. The boundary layer solution was obtained by using the experimental surface Mach number distribution as input data. Therefore, it can be regarded as a good reference for our results. But they are definitely not the experimental data, and we believe the present results are more accurate than the boundary layer solution.

It is well known that skin friction is much more sensitive to the grid resolution than other flow quantities. Figures 7 and 8 show the skin friction coefficient distributions on the pressure and suction surface obtained with the present k–ω model on different sizes of grids. The results obtained on 160×64, 192×80, 224×97 collapse onto each other. We can safely conclude that the grid of 192×80 provides enough grid resolution.

It is worth mentioning that if only the TSL modification is used, the small hump in the isentropic Mach number distribution is not captured because the flow on the suction surface will not undergo

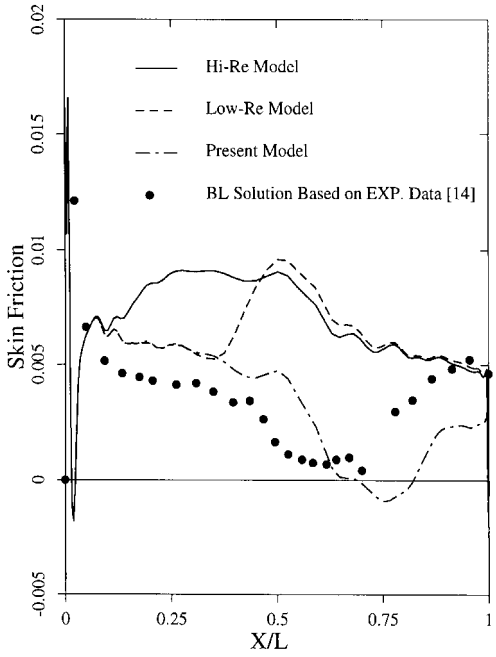

Figure 5. Skin friction coefficient distribution on suction surface, design condition

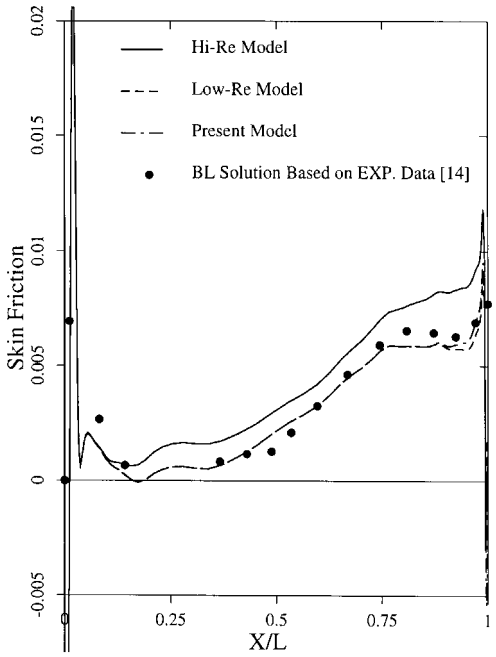

Figure 6. Skin friction coefficient distribution on pressure surface, design condition

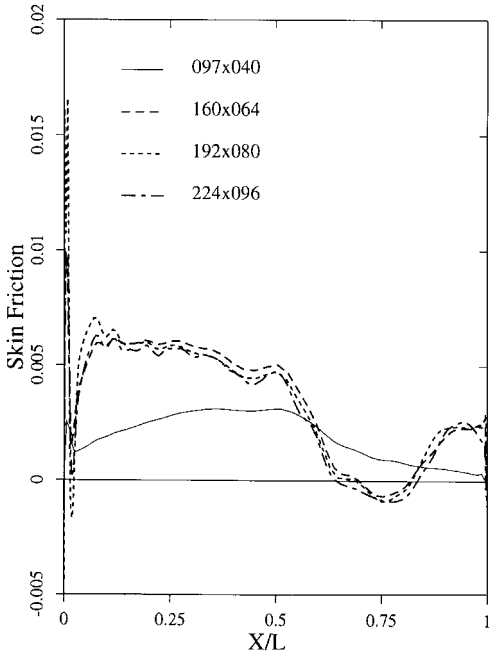

Figure 7. Skin friction obtained on different grids (suction surface, design condition)

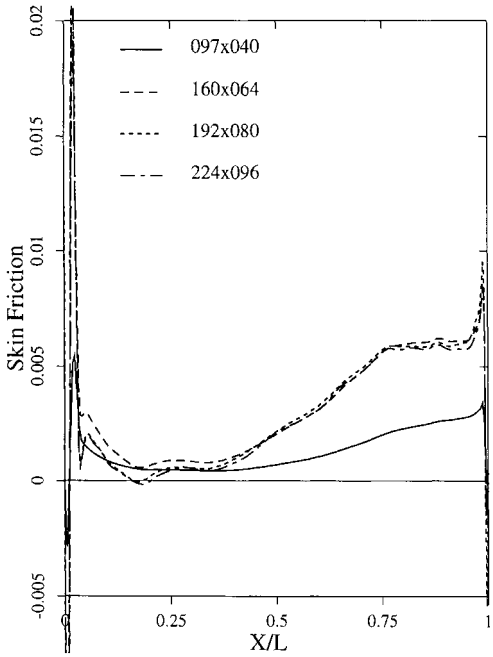

Figure 8. Skin friction obtained on different grids (pressure surface, design condition)

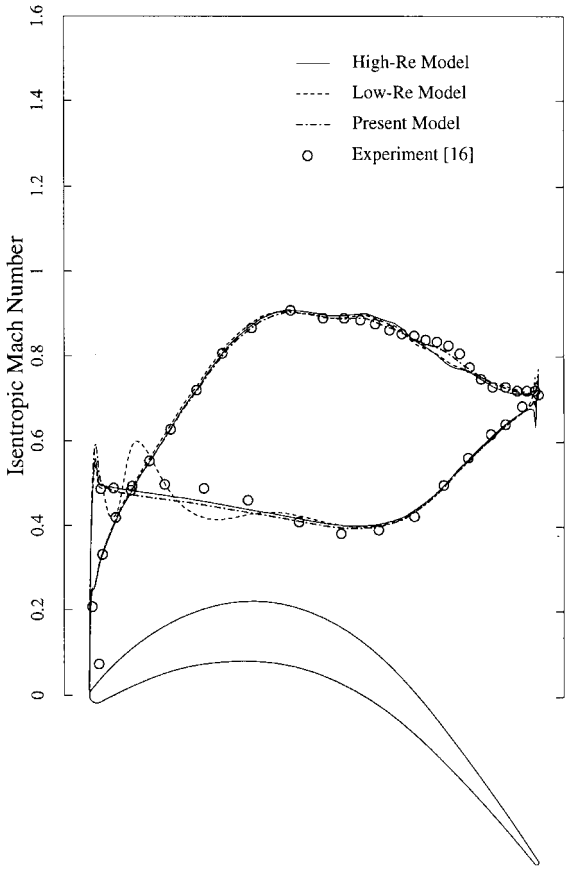

Figure 9. Isentropic Mach number distribution at off-design condition

transition at all, even after separation. It should be noted that the actual separation strength is much stronger than that of purely laminar separation. Here, the laminar separation triggers turbulent transition, and in return, the turbulent flow pushes back with greater momentum and therefore further strengthens the separation. With out transition, the separation strength of laminar flow is not strong enough to make the isentropic Mach number distribution curve-up, and no curve-down will be followed since there is no re-attachment.

Figures 9–11 show the corresponding results for an off-design condition. In this case, the incoming flow has a negative incidence angle of 20·3° relative to the design condition. This large incidence angle leads to a big separation bubble near the pressure surface. The calculation with the original high-Reynolds-number k–ω model continues to miss the small hump on the suction surface, but the large separation bubble on the pressure surface is predicted with reasonable accuracy as shown in Figure 9.

We were unable to achieve a converged steady solution for this case with use of the low-Reynolds-number k–ω model. This model fails to predict the transition immediately after separation near the pressure leading edge. Although a large separation bubble is found on the pressure surface,

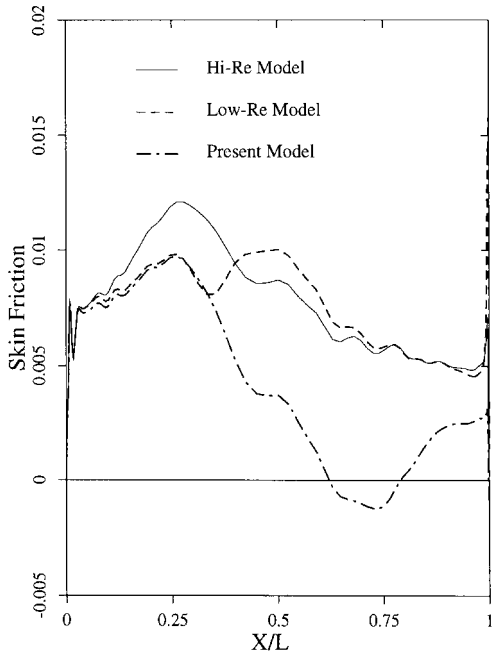

Figure 10. Skin friction coefficient distribution on suction surface, off-design condition

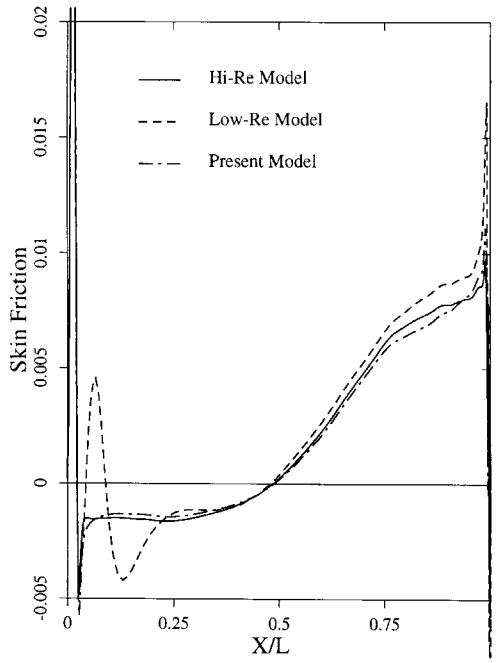

Figure 11. Skin friction coefficient distribution on pressure surface, off-design condition

it is a fully laminar one, and no steady solution can be reached. This case fully demonstrates the dilemma faced by most low-Reynolds-number models, i.e. too early transition is predicted for attached flows like on the suction surface, and too late transition for separated flows as predicted here on the pressure surface. The result shown in Figure 10 for the low-Reynolds-number k–ω model is only a solution at one instant.

With use of the modified low-Reynolds-number k–ω model, both the large separation bubble on the pressure surface, and the tiny separation bubble on the back of the suction surface are predicted accurately. The small hump is fully captured.

The main objective of this work was to develop a transitional two-equation model, and so no effort was made to improve the performance of two-equation model in the fully turbulent flow region. As can be seen in Figure 11, a noticeable difference between calculated isentropic Mach number and experimental data was found on the pressure (lower) surface in common with the original high-Reynolds-number model (Figure 9). The slight difference between Figures 9 and 11 is caused by the different transition features of these two models.

The skin friction coefficient distributions calculated by the three models are displayed in Figures 10 and 11. Neither experimental data, nor numerical results from other methods are available for this case. These plots serve to demonstrate how significantly different the results can be when using different turbulence models, and how important the transitional model is for practical applications.

8. CONCLUDING REMARKS

Two novel modifications for a two-equation model have been described which improve the prediction of flows undergoing turbulent transition. The first modification uses the total-stress-limitation concept to improve prediction of high Reynolds number transition. The second modification introduces a separation sensor to automatically detect the separation zone and trigger the turbulent transition. The present modifications are only active in transitional regions. No effort is made to improve the k–ω model in fully turbulent regions.

The low-pressure turbine cascade cases are generally believed to be difficult cases for low-Reynolds-number turbulence models. Multiple points of separation, transition and relaminarization provide a severe test for the transitional model. The flows on pressure surface and suction surface are so different that each side can be considered as a test case for the present transitional model. Although the performance of the modified model is very good, there is scope for improvement, and we anticipate greater success of two-equation turbulence models in prediction of flow transition.

REFERENCES

1. C. Liu and Z. Liu, 'Multigrid mapping and box relaxation for simulation of the whole process of flow transition in 3-D boundary layers', *J. Comput. Phys.*, **119,** 325–341 (1995).
2. Z. Liu, G. Xiong and C. Liu, 'Direct numerical simulation for the whole process of transition on 3-D airfoils', *AIAA Paper 96-2081*, June 1996.
3. A. M. O. Smith and N. Gamberoni, 'Transition, pressure gradient and stability theory', *Douglas Aircraft Co. Report ES 26388*, EL Segundo, California, 1956.
4. J. L. Van Ingen, 'A suggested semi-empirical method for the calculation of the boundary layer transition region', *Report UTH-74*, Department of Aerospace Engineering, University of Technology, Delft, 1956.
5. G. Casalis, M. L. Copie, Ch. Airiau and D. Arnal, 'Nonlinear analysis with PSE approach', in P. W. Duch and P. Hall (eds.), IUTAM Symp. on Nonlinear Instability and Transition in Three-Dimensional Boundary Layers, Kluwer Academic Publishers, Dordrecht, 1996, pp. 237–246.

6. D. Arnal, G. Casalis and J. C. Juillen, 'A survey of the transition prediction methods: from analytical criteria to PSE and DNS', in M. Hallback (ed.), *Turbulence and Transition Modelling*, Lecture Notes from the ERCOFTAC/IUTAM Summer School Held in Stockholm, 12–20 June 1995, Kluwer Academic Publishers, Dordrecht, 1996, pp. 3–14.
7. J. Steelant and E. Dick, 'Modelling of bypass transition with conditioned Navier–Stokes equations coupled to an intermittency transport equation', *Int. J. Numer. Meth. Fluids*, **23,** 193–220 (1996).
8. E. Dick and J. Steelant, 'Coupled solution of the steady compressible Navier–Stokes equations and the k–ε turbulence equations with a multigrid method', *Appl. Numer. Math.*, **23,** 49–61 (1997).
9. R. C. Schmidt and S. V. Patankar, 'Simulating boundary layer transition with low-Reynolds number k–ε turbulence models: Part 1—an evaluation of prediction characteristics', *J. Turbomachinery*, **113,** 10–17 (1991).
10. D. C. Wilcox, 'Simulation of transition with a two-equation turbulence model', *AIAA J.*, **32**(2), 247–255 (1994).
11. X. Zheng and F. Liu, 'Staggered upwind method for solving Navier–Stokes and k–ω turbulence model equations', *AIAA J.*, **33**(6), 991–998 (1995).
12. X. Zheng, C. Liao, C. Liu, C. Sung and T. Huang, 'Multiblock multigrid incompressible flows using two-equation turbulence models', *AIAA Paper 97-0626*, January 1997.
13. D. C. Wilcox, 'Alternative to the e^9 procedure for predicting boundary-layer transition', *AIAA J.*, **19**(1), 56–64 (1981).
14. H. P. Hodson, 'Boundary layer transition and separation near the leading edge of a high speed turbine blade', *ASME Paper 84-GT-179*. Also in *ASME J. Engng. Gas Turbines Power*, **107,** (1985).
15. H. P. Hodson and R. G. Dominy, 'Three-dimensional flow in a low pressure turbine cascade at its design condition', *ASME Paper 86-GT-106*, 1986. Also in *ASME J. Turbomachinery*, **109,** 177–185 (1987).
16. H. P. Hodson and R. G. Dominy, 'The off-design performance of a low pressure turbine cascade', *ASME Paper 86-GT-188*, 1986. Also in *ASME J. Turbomachinery*, **109,** 201–209 (1987).
17. F. Liu and X. Zheng, 'A staggered finite volume scheme for solving cascade flow with a two-equation model of turbulence', *AIAA J.*, **32**(8), 1589–1597 (1994).
18. P. L. Roe, 'Approximate Riemann solvers, parameter vectors, and difference schemes', *J. Comput. Phys.*, **43**(3), 357–372 (1981).
19. A. Jameson, W. Schmidt and E. Turkel, 'Numerical solutions of Euler equations by finite volume methods using Runge–Kutta time-stepping schemes', *AIAA-81-1259*, 1981.
20. F. Liu and X. Zheng, 'A strongly coupled time-marching method for solving the Navier–Stokes and k–ω turbulence model equations with multigrid', *J. Comput. Phys.*, **128,** 289–300 (1996).
21. F. R. Menter, 'Influence of freestream values on k–ω turbulence model predictions', *AIAA J.*, **30**(6), 1657–1659 (1992).
22. D. C. Wilcox, 'Reassessment of the scale-determining equation for advanced turbulence models', *AIAA J.*, **26**(11), 1299–1310 (1988).
23. D. C. Wilcox, 'A half century historical review of the k–ω model', *AIAA 91-0615*, 1991.

